An Experimental Investigation of the Interaction between a Transverse Sonic Jet and a Hypersonic Stream

V. ZAKKAY,* W. CALARESE,† AND L. SAKELL†
New York University, Bronx, N. Y.

The interaction of an underexpanded jet with a hypersonic stream is studied. The investigation includes an experimental study of a finite span sonic jet on a 7°-semivertex angle sharp cone in a Mach number 5.8 stream. A range of unit Reynolds numbers of 2×10^6 to 4×10^7/ft is covered in the experiments, producing laminar, transitional and fully turbulent boundary layers on the conical surface. The models are instrumented with 60-surface pressure taps from which data on normal force coefficients are derived. In addition, the resultant forces are checked with a strain balance. Shock-wave and streamwise patterns in the plane of symmetry of the flowfield are obtained from Schlieren photographs. The experimental study is primarily intended to provide quantitative data on interaction forces due to the three-dimensional effects of a finite span jet. It is observed in these experiments that the cross flow can produce a favorable net interaction with the mainstream, thereby providing an induced normal force coefficient equal to or possibly exceeding the two-dimensional values, at the same Mach number and jet mass flux ratio. The experimental data show that a positive normal force (lift) contribution can be obtained from the flow downstream of the jet slot. Finite span fences have been tested for comparison with jet controls. It is found that the total normal force coefficient produced by the jet for which the Mach disk penetrates the flowfield to the same height as the fence is much larger than that produced by the fence.

Nomenclature

A = surface area
A_{ref} = reference area $[(\phi/360°)\pi L^2 \sin\eta]$
b = slot span
C_{NA} = normal force coefficient, $2\int_A (P - P_i) \cos\varphi \cos\eta dA/\rho_\infty U_\infty^2 A_{ref}$ where φ = semispan angle
C_{NR} = thrust coefficient $2T/\rho_\infty U_\infty^2 A_{ref}$
d = slot width
F_i = normal force due to interaction with a forward-facing step or transverse fence
F_{NA} = normal force due to jet interaction
h = step or fence height, or height of Mach disk above the surface
l = length of separated flow region
L = surface length from cone apex to slot or fence
M = Mach number
P = static pressure
P_0 = total pressure
r = radius of cross-sectional area at slot location
R = gas constant
Re = Reynolds number, $\rho ux/\mu$
S = surface length from slot or fence position
T = thrust, or static temperature
T_0 = total temperature
u = streamwise component of velocity
$\dot{w}$ = mass flux
x = streamwise or axial coordinate
δ = boundary-layer thickness
γ = ratio of specific heats
η = cone semivertex angle
μ = viscosity
ρ = density
θ = momentum defect thickness
θ_s = separation shock angle
φ = meridional angle ($\varphi = 0$ being the symmetry plane) semispan angle
Φ = total span angle (deg)

Subscripts

c = conical, cone surface value
e = boundary-layer edge
i = initial or undisturbed cone surface value
j = jet
w = wall or surface value
∞ = freestream conditions, ahead of the separated region
2D = two-dimensional
3D = three-dimensional
bl = boundary layer
$\mathfrak{L}$ = centerline
sp = separation point
tr = transition point
θ = based on momentum thickness
t_∞ = freestream conditions

Received August 9, 1968; revision received August 19, 1970. This work was supported by the Aerospace Research Laboratories, Office of Aerospace Research, U.S.A.F., Wright-Patterson Air Force Base, Ohio, under contract F33615-68-C-1184.

* Professor, Department of Aeronautics & Astronautics.
† Assistant Research Scientist, Department of Aeronautics & Astronautics.

I. Introduction

SECONDARY jets have received attention as a possible, alternative to conventional aerodynamic surfaces (e.g., ailerons, flaps, flares, etc.) for supersonic or hypersonic flight control systems. The forces generated by an underexpanded jet issuing normal to a surface are known to be amplified considerably over the in-vacuo thrust of the jet, due to a complex interaction with the main, supersonic stream. Also, the severe heating and loading problems associated with the exposure of a control surface to a supersonic or hypersonic stream may be avoided. These considerations have motivated a number of investigations of the "jet interaction" phenomenon, and have renewed (or expanded) the interest in boundary-layer separation and reattachment and jet plumes.[1-11]

The structure of the two-dimensional jet-interaction flowfield has been inferred by a number of investigators, from Schlieren photographs, and surface pressure distributions. There appears to be a general consensus of opinion about the general features of the flowfield, although some disagree-

ment has arisen in regard to the effects of various parameters on its structure and the resultant forces.[11] It should also be pointed out that the structure is usually depicted for a jet that penetrates into the stream to a height many times the thickness of the upstream boundary layer. A somewhat different behavior pertains to the case where the penetration height is of the same order as the boundary-layer thickness. The case where the boundary layer is very thin is shown schematically in Fig. 1, which is based on features observed in Schlieren photographs and surface dye patterns.[14]

The jet interaction flowfield of a finite-span jet, on the other hand, is essentially three-dimensional. In fact, only an axially-symmetric body (at zero angle of attack) can assuredly produce a two-dimensional flow[4]; with a planar geometry, spurious three-dimensional effects can be subtle and difficult to eliminate. Spaid and Zukoski[10] attribute the relative reduction in amplification of two-dimensional jet interaction forces with increasing ratio of jet to main stream total pressure to three-dimensional effects rather than any basic dependence of the amplification factor on this parameter. It is implied that the three-dimensional effects associated with finite-span jets can reduce the beneficial induced forces; indeed, on a conical body circumferential crossflow may nearly cancel the induced normal force. The present experimental investigation is primarily concerned with the three-dimensional problem of a finite-span jet or a forward facing fence on a conical body. The results of an experimental study are presented, and compared with previous data regarded as two dimensional.

The need for a detailed analysis of the flowfield, particularly in the three-dimensional case, is considered apparent. In Ref. 14, a new theoretical approach has been developed, based on an inviscid, rotational flow model.

II. Experimental Investigation

A. Experimental Apparatus and Test Conditions

All the tests were conducted in the NYU blowdown-type tunnel equipped with a nominal Mach 6 axially symmetric contoured nozzle. The test section is 1 ft in diam and consists of a uniform flow 9 in. in diam and 3 ft in length. The tunnel stagnation temperature was 820°R in all the tests, and the stagnation pressure was varied from 1800 psia to 60 psia.

The models used were two-sharp cones of 7° semivertex angle. One had a base diameter of 4.60 in. and the other of 3.52 in. The over-all surface length was respectively 19.0

Table 1 Symbols for jet injection tests (unshaded symbols refer to pressure measurements, shaded symbols refer to balance measurements). Pressures are measured in pounds per square inch

a) SPAN = 60°, L = 14.25", d=0.015"

P_{o_∞}	P_{o_j}	$P_{o_j}d/P_{o_\infty}$	L (x10⁴)	SYMBOL
1733	100	0.577		

b) SPAN = 60°, L = 14.25", d=0.030"

P_{o_∞}	P_{o_j}	$P_{o_j}d/P_{o_\infty}$	L (x10⁴)	SYMBOL
60	90	31.5		
100	90	18.9		
200	90	9.45		
160	70	9.18		
305	90	6.19		
200	45	4.72		
400	90	4.72		
200	23.5	2.46		
400	45	2.36		
800	90	2.36		
203	12	1.24		
400	23.5	1.23		
800	45	1.18		
1830	100	1.15		
1800	90	1.05		

c) SPAN = 30°, L = 12.25", d= 0.01"

P_{o_∞}	P_{o_j}	$P_{o_j}d/P_{o_\infty}$	L (x10⁴)	SYMBOL
100	103	8.46		
210	150	5.87		
150	100	5.47		
210	100	3.91		
410	150	3.0		
360	103	2.35		
700	103	1.20		

d) SPAN = 60°, L = 12.25", d= 0.01"

P_{o_∞}	P_{o_j}	$P_{o_j}d/P_{o_\infty}$	L (x10⁴)	SYMBOL
220	100	3.73		
210	50	1.95		
420	100	1.95		
410	78	1.56		
740	100	1.11		
430	50	0.955		
730	80	0.895		
730	51.7	0.582		
740	35	0.388		
730	30	0.337		

e) SPAN = 90°, L = 12.25", d= 0.01"

P_{o_∞}	P_{o_j}	$P_{o_j}d/P_{o_\infty}$	L (x10⁴)	SYMBOL
105	100	7.82		
150	100	5.47		
310	100	2.64		
710	101.25	1.16		
410	52	1.03		
300	33.75	0.92		
710	67.5	0.78		
720	33.75	0.384		

f) SPAN = 150°, L = 12.25", d= 0.01"

P_{o_∞}	P_{o_j}	$P_{o_j}d/P_{o_\infty}$	L (x10⁴)	SYMBOL
100	100	8.22		
210	100	3.91		
310	100	2.64		
210	32	1.25		
410	32	0.649		
700	32	0.375		

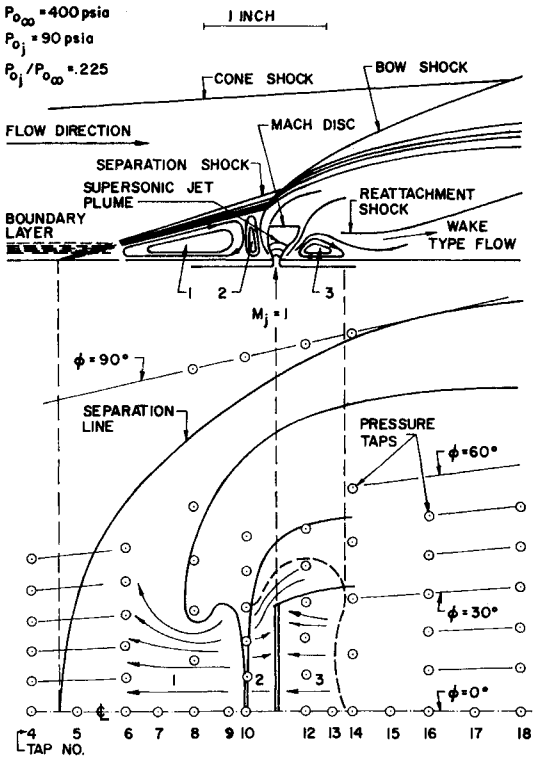

Fig. 1 Schematic of flowfield in the plane of symmetry and surface streamline pattern.

in. and 14.47 in. A slot was machined normal to the surface of the cones at axial stations of 14.15 in. and 12.16 in. from the tip. Different slot widths were used, namely 0.01 in., 0.015 in., and 0.030 in. The spans of the slots were also varied. Peripheral span angles of 30°, 60°, 90°, and 150° were used. The complete inner chamber of the models was used as the stagnation chamber for the jet. The wall temperature of the models was constant at about 520°R.

The jet mass flux was measured with a venturi nozzle and compared with the theoretical mass flux through the jet slot, and the discharge coefficient was approximately 0.95. For the experiments with solid fences, the fences were installed normal to the cone surface at the same location as the jet. The larger diameter cone was equipped with 60 pressure taps, and the pressure distributions over the conical surface were measured by two-scannivalve transducers. The normal and axial forces were computed by numerical integration of the measured pressure distributions. The smaller diameter cone was equipped with a 3-component strain gauge balance and the normal and axial forces, as well as pitching moments, were measured directly.

The nature of the boundary layer on the cone surface without injection was determined for the full range of stagnation conditions by heat-transfer measurements. For the present test conditions all the data can be correlated by

$$Re_\theta = 0.4(\rho_e u_e x_{TR}/\mu_e)^{1/2}$$

and a value of $Re_\theta = 750$ was obtained over the full range of stagnation conditions. Transition occurs (naturally) within an inch of the cone apex at the highest P_{0_∞} (1800 psia); whereas a completely laminar boundary layer persists over the entire cone surface at the lowest P_{0_∞} (60 psia). Thus, a wide range of the parameter P_{0_j}/P_{0_∞} was attainable with laminar, transitional and fully turbulent boundary layers (without artificial trips).

Table 1 presents a list of symbols corresponding to the various experiments performed.

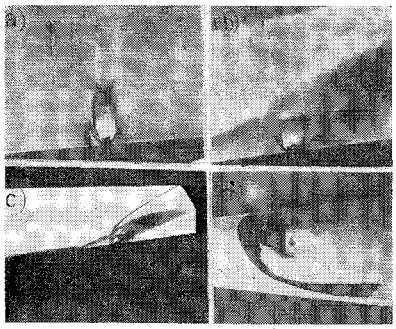

Fig. 2 Schlieren photos of jet interaction flowfield and pictures of ink pattern of model surface: a) $P_{o\infty} = 0$; $P_{oj} = 90$ psia, b) $P_{o\infty} = 400$ psia; $P_{oj} = 90$ psia, c) $P_{o\infty} = 400$ psia; $Po_j = 90$ psia; and d) $Po_\infty = 400$ psia; $Po_j = 90$ psia.

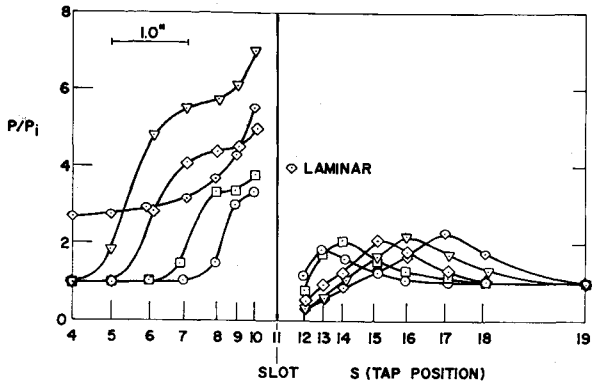

Fig. 3a Surface pressure distribution along plane of symmetry for jet interaction.

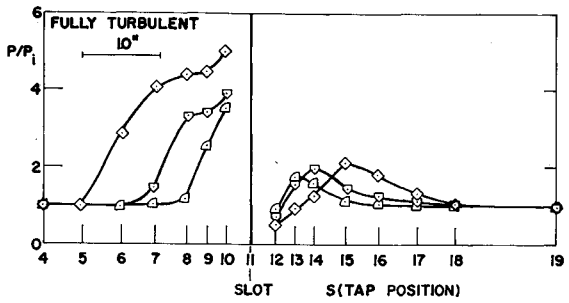

Fig. 3b Surface pressure distribution along plane of symmetry for different pressure ratios: turbulent flow; $P_{o\infty} = 400$ psia, $Re/\text{ft} = 8.4 \times 10^6$.

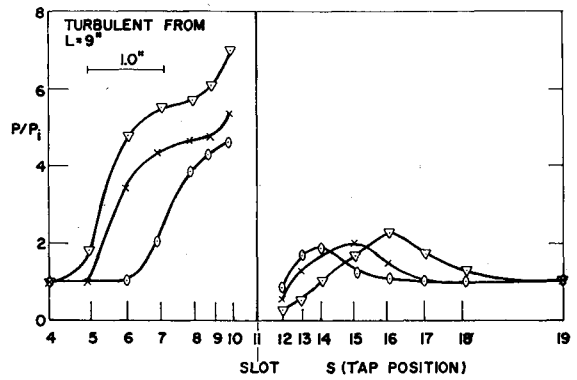

Fig. 3c Surface pressure distribution along plane of symmetry for different pressure ratios: turbulent flow from $L = 9$ in., $P_{o\infty} = 200$ psia; $Re/\text{ft} = 4 \times 10^6$.

B. Experimental Results: Finite-Span Jet

The experiments with a finite-span jet were performed at $M_{t\infty} = 5.8$ and $M_j = 1$. The data obtained include surface pressure distributions in the plane of symmetry (normal to the jet slot) and in transverse planes both upstream and downstream of the jet slot, balance measurements, Schlieren photographs (viewing the pitch plane, a plane of symmetry in the present experiments), and surface dye patterns. (The dye is an ink/alcohol mixture that was injected through a surface tap in the recirculation region.)[14] For example, an enlargement of the Schlieren photo of the jet interaction flowfield shown in Fig. 2b provided the basis of the schematic diagram in Fig. 1. The surface dye pattern shown in Fig. 2d led to the surface streamline pattern also illustrated in Fig. 1. Typical surface pressure distributions in the plane of symmetry are presented in Figs. 3a–3e, and in transverse

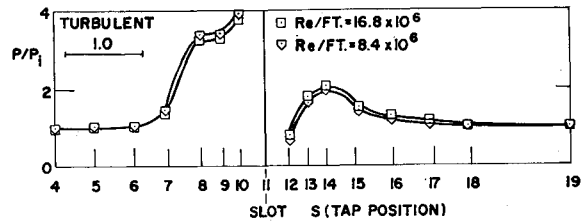

Fig. 3d Surface pressure distribution along plane of symmetry for different Re: turbulent flow; $P_{oj}/P_{o\infty} = 0.112$.

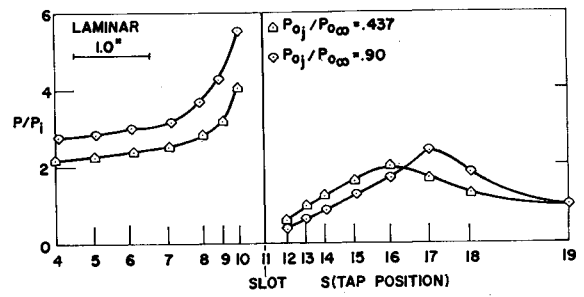

Fig. 3e Surface pressure distribution along plane of symmetry for different pressure ratios: laminar flow; $P_{o\infty} = 100$ psia; $Re/\text{ft} = 2 \times 10^6$.

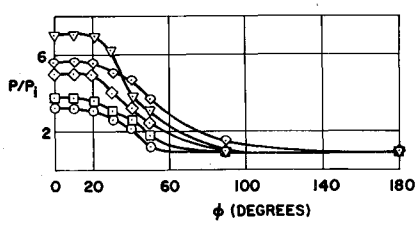

Fig. 3f Transverse distribution of surface pressure at $L = 14.0$ in.

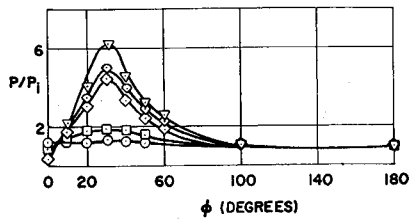

Fig. 3g Transverse distribution of surface pressure at $L = 14.5$ in.

planes upstream and downstream of the slot in Figs. 3f and 3g, respectively.

The various pressure distributions are functions of jet to freestream pressure ratio, Reynolds number, turbulent or laminar flows. Figs. 3a–3e show that the pressure distributions are strong functions of P_{0_j}/P_{0_∞} and weak functions of Reynolds number. They increase considerably with P_{0_j}/P_{0_∞} and decrease slightly with increasing Reynolds number. This behavior applies to both turbulent and laminar flows. It is interesting to compare turbulent and laminar separations. The turbulent separation gives rise to a greater plateau pressure for the same P_{0_j}/P_{0_∞}. But the laminar separation, not being able to withstand the same pressure rise, occurs much earlier that the turbulent one.

A set of Schlieren photos for various P_{0_∞} and P_{0_j} are shown in Figs. 4a–4g and tracings of separation lines obtained from ink patterns[14] in Fig. 5. The plume of the jet at $P_{0_j} = 90$ psia into a quiescent atmosphere at the same static pressure (less than 1 psia) that occurs behind the cone shock at $M_{t_\infty} = 5.8$ and $P_{0_\infty} = 400$ psia is shown in Fig. 2a. Comparison with the plume in Fig. 2b shows clearly how the jet structure is grossly altered by the oncoming stream. Thus, although the jet acts like a protrusion or a step that deflects the mainstream, the height to which it penetrates the flowfield is the result of a mutual interaction between the streams that includes significant effects of crossflow in the present experiments. The strong shock (or "Mach disk") through which the central core of the jet passes is evident in the Schlieren pictures, although it must be borne in mind that only the plane of symmetry is visible. The height and shape of the shock near the ends of the jet slot were not observed. It is also noted that as the plume is pushed rearward by the mainstream, the "Mach disk" may become oblique to the flow in the jet core, although the shock remains nearly parallel to the cone surface. Thus, the flow downstream of the "Mach disk" need not be subsonic, as often assumed.

The existence of two distinct, separate bubbles of counter-rotating flow upstream of the jet was confirmed by injection of dye in region 1 of Fig. 1, where it flowed upstream, and injection in region 2, where it flowed downstream. This behavior was most clearly evident at the higher values of

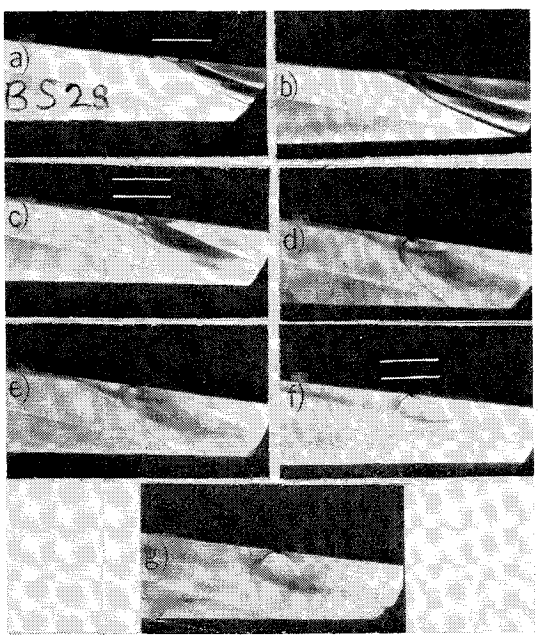

Fig. 4 Schlieren pictures of interaction of finite jets for various jet to freestream stagnation conditions: a) $P_{0_\infty} = 1800$: $P_{0j} = 90$, b) $P_{0_\infty} = 800$: $P_{0j} = 90$, and c) $P_{0_\infty} = 420$: $P_{0j} = 90$, d) $P_{0_\infty} = 200$: $P_{0j} = 90$, e) $P_{0_\infty} = 160$: $P_{0j} = 70$, f) $P_{0_\infty} = 100$: $P_{0j} = 90$, and g) $P_{0_\infty} = 60$: $P_{0j} = 90$.

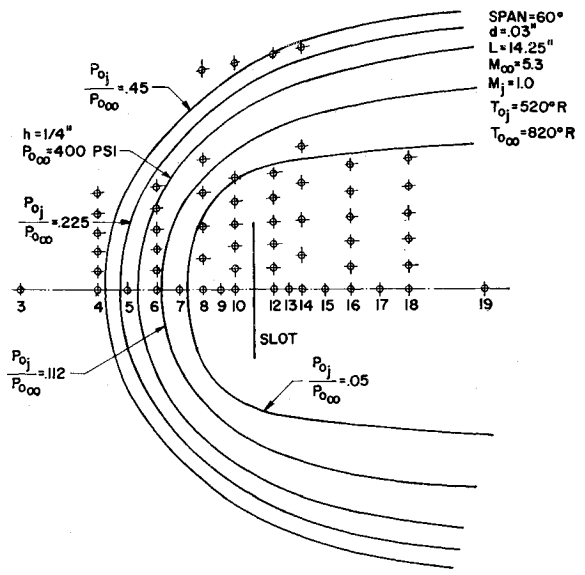

Fig. 5 Separation lines obtained from ink pattern tracings.

P_{0_j}/P_{0_∞} (e.g., see Fig. 2d and Fig. 1, which was traced from the model).

It is of interest to compare the geometry of the turbulent separated flow region in the plane of symmetry of the present experiments with previous results for nearly two-dimensional flows,[2,3] (the data of Ref. 2 will be considered here as quasi two dimensional, since the side plates were placed 1 in. from a slot span of 8 in.).

In correlating the present experimental data, and in comparing the results of Ref. 2, one must be careful in the proper choice of the similarity parameter.[12] There has been a controversy over the nondimensionalizing quantities for this type of jet interaction. Reference 2, as well as others,[7–13] has chosen to nondimensionalize his quantities with respect to L; whereas others, such as Ref. 10, have chosen the slot span b. It is felt here that both L and b for two-dimensional work are not the proper quantities, since for a turbulent boundary layer the jet interaction effects are almost independent of L, and the two-dimensional nature of the jet is practically independent of b. It will be shown later that b is also a poor choice for three-dimensional interaction.

In order to correlate the present data, the mass flow per unit span has been taken, i.e., jets are compared for the same mass flow issuing from the slot and referenced to the surface area subtended by the slot. The results of such a correlating parameter indicate that for the same Mach number ahead of the interaction region $[(P_{0_j}/P_{0_\infty})d/L]$ would be the proper choice for three-dimensional work (P_{0_∞} refers to conditions just ahead of the separation region, as the conical values with no interaction in this case). The results of the present experiment as well as other three-dimensional works will be shown to correlate in this manner. The problem arises, using the present correlating parameter, when comparisons between quasi two-dimensional work and the present three-dimensional results are made. In order to make a meaningful comparison, the dependence on L must be taken out by nondimensionalizing all the values with respect to the same value of L.

The jet penetration height h/L, and the length of the separated flow region l/L for various values of $(P_{0_j}/P_{0_\infty})d/L$ are presented in Fig. 6. Included in the figure are the experimental results of Ref. 2. Since L for Ref. 2 is 19.25 in., the results have been nondimensionalized with respect to $L = 14.25$ in. In this manner, the dependence on L has been taken out. Figure 6 gives also the angle between the wall and the line from the separating point to the top of the Mach disk. For the conditions corresponding to Fig. 1, l/h of 5.3

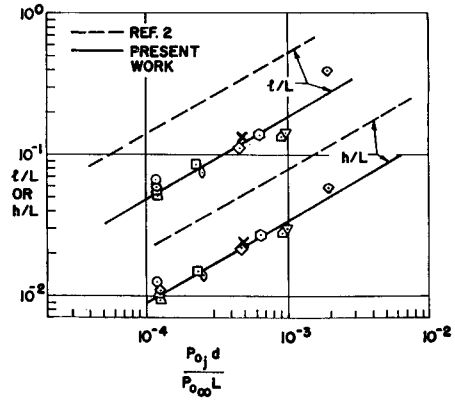

Fig. 6 Separation distance and jet penetration height.

is obtained for the present experiments, which yields a corresponding separation angle of about 10°. The data of Ref. 2, although having the same power law variation with $(P_{0_j}/P_{0_\infty})(d/L)$, give an l/h of 6.2, with a corresponding separation angle of about 9.5°. Application of two-dimensional oblique shock relations locally in the plane of symmetry for the present experimental conditions gives a separation shock angle of about 20° and a plateau pressure of $P_e/P_i = 3.7$. This shock angle is within 1° of that which can be measured from the Schlieren photo. The observed pressure ratio is about 4.2 (see Fig. 3a). The jet penetration height is 0.295 in., giving a jet aspect ratio (b/h) of 6.1, which is apparently sufficient to produce a locally two-dimensional flow in the plane of symmetry. However, it should be noted that this comparison has been made in terms of the jet penetration height as a scale factor for the separated region; the jet mass flux necessary to achieve a given penetration height is much larger in the present experiments than in two-dimensional flows. This can be seen in Fig. 6 where the present data are compared to the quasi-two-dimensional results of Ref. 2. The three-dimensional results indicate that 3 to 4 time the jet mass flux must be expended to achieve a comparable penetration height as the results of Ref. 2. This behavior is clearly attributed to the effects of crossflow. The low energy flow diverts laterally around the finite-span jet, which therefore, faces an effectively more energetic stream. For the experiments of Ref. 2, since the fences were placed 1 in. from the end of an 8-in. slot, the three-dimensional relief is small in comparison to the results presented here, where for some of the tests, a three-dimensional relief of as much as twice the length of the slot was obtained (see Fig. 5).

The normal force coefficient C_{N_A} is obtained by nondimensionalizing the total normal force acting on the surface of the cone with respect to the freestream dynamic pressure and the surface area of the sector of the cone intercepted by the jet slot (that is $\frac{1}{6}$ of the total surface area up to the jet location for $\Phi = 60°$). In this form the C_{N_A} is comparable to the C_{N_A} per unit span for 2-D flows. It is noted that different spans for the slot (up to 180°) might be chosen for the experiment. Contrary to the 2-D case, where a unit span can be chosen without affecting the value of C_{N_A}, in

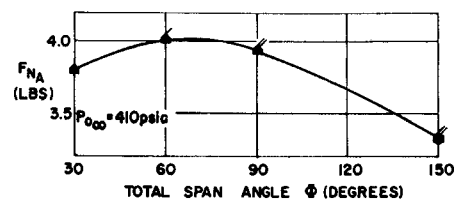

Fig. 7 Normal force dependence on jet slot total span angle for constant mass flow.

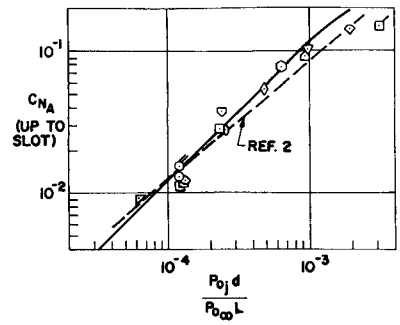

Fig. 8 Normal force coefficient measured up to the jet slot.

the 3-D case the span might have a direct effect on C_{N_A} due to the lateral dissipation.

In order to find the span that would give the maximum value of C_{N_A}, experiments were performed varying the span of the slot while keeping the mass flux constant. A plot of F_{N_A} vs a slot span for constant mass flux (Fig. 7) showed that the best interaction is achieved using a 60° span. The reason for this behavior is due to the fact that for a slot span less than 60°, the obstacle encountered by the main stream is too small to have a strong effect on the interaction, and for a slot span of over 60°, the normal force component is considerably reduced due to the separated region extending beyond $\varphi = 90°$, thus producing a counteracting force on the opposite side of the cone.

The normal force coefficient obtained by integration over the surface area up to the jet slot location is plotted in Fig. 8 as a function of the jet mass flux parameter $P_{0_j}d/P_{0_\infty} L$ for $L = 14.25$ in., $\Phi = 60°$.

The results of Ref. 2, which are also obtained by integrating the pressure distribution up to the slot, are also included in Fig. 8, and the agreement is considered good. The results obtained by integration of the pressure distribution over the entire cone surface, for $L = 14.25$ in., $\Phi = 60°$ are presented in Fig. 9. Included in the same figure are the results of the balance measurements for $L = 12.25$ in., $\Phi = 60°$, and the agreement is satisfactory. The results for various spans taken with the balance for $L = 12.25$ in. are presented in Fig. 10. C_{N_A} is weakly dependent on the choice of the span b, but attains the maximum value for $\Phi = 60°$. If we were to nondimensionalize the parameter $P_{0_j}d/P_{0_\infty}$ with respect to b, the value of C_{N_A} would be maximum for $\Phi = 150°$, as it can be readily verified, and it would be strongly dependent on the choice of b. This would contradict the experimental results (see Fig. 7).

The data for C_{N_A} over the entire cone surface show a consistently higher normal force (about 70%) than those which include only the interaction upstream of the jet slot (compare Figs. 8 and 9). They are also adequately correlated as a linear function of $P_{0_j}d/P_{0_\infty}L$, although the data at the highest jet mass flux ratios show a nonlinear behavior. It can be deduced that the linear behavior of C_{N_A}, computed using a 60° span, is limited to a jet mass flux parameter $(P_{0_j}d/P_{0_\infty}L)$ of up to 10^{-3} or $P_{0_j}/P_{0_\infty} \approx 0.45$ for $d = 0.03$ in. and $L = 14.25$ in. This is confirmed by the behavior of the

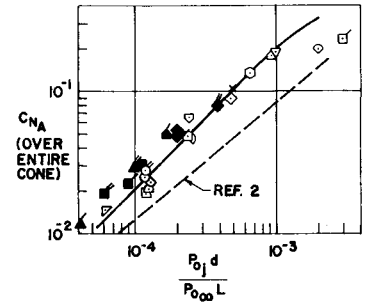

Fig. 9 Normal force coefficient measured over entire cone surface.

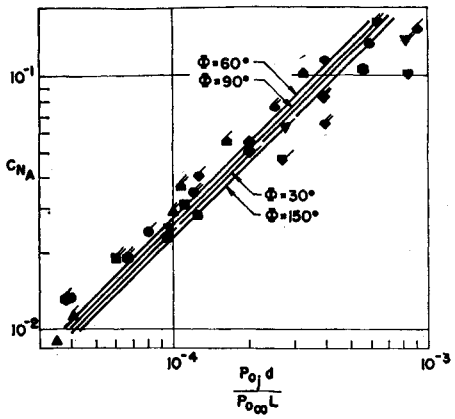

Fig. 10 Normal force coefficient obtained from balance measurements for various jet slot spans.

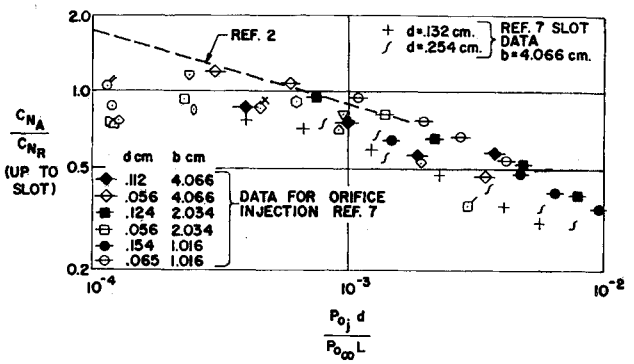

Fig. 11 Normal force amplification ratio, measured up to the jet slot.

separation streamlines shown in Fig. 5. The experimental points for $P_{0_j}d/P_{0_\infty}L > 10^{-3}$ in Figs. 8 and 9 refer to laminar flow. For values of $P_{0_j}d/P_{0_\infty}L \ll 10^{-3}$, the C_{N_A} for laminar conditions is greater that the turbulent C_{N_A}, because although the pressure rise in the separated region is less for laminar than for turbulent flow, the surface area of the separated region is greater. However, for $P_{0_j}d/P_{0_\infty}L > 10^{-3}$, the laminar separation region goes beyond $\varphi = 90°$ at a greater rate than in the turbulent case and therefore C_{N_A} laminar $< C_{N_A}$ turbulent.

From the figures presented so far it is evident that a positive normal force (lift) contribution is obtained from the flow downstream of the jet. Regions of both negative lift ($P < P_i$) and positive lift ($P > P_i$) are found downstream of the jet (see e.g., Figs. 3a–3e and 3g), whereas only positive lift is obtained upstream of the jet (see e.g., Figs. 3a–3f). The relative magnitude of the positive and negative contributions downstream of the jet evidently depends on several factors: namely, the strength of the recompression shock where the flow reattaches to the surface and the lateral extent of the crossflow effects beyond the jet. In the present experiments recompression pressures of twice the undisturbed conical values are obtained in some case. Spaid and Zukoski[10] observed a recompression pressure ratio of about 1.5 at $M_\infty = 4.5$, with zero net normal force contribution from this region, whereas at $M_\infty = 3.4$ and 2.6 they report a negative net contribution. These results imply that the relative importance of the positive and negative lift contributions downstream of the jet just cancel each other at $M_\infty \approx 4.5$, and the positive part becomes progressively more dominant as M_∞ increases.

Another comparison between the effectiveness of two-dimensional and three-dimensional jet control interaction can be made in terms of the force amplification ratio:

$$C_{N_A}/C_{N_R} = \int_A (P - P_i) \cos\varphi \cos\eta dA/T$$

where the normal component of the jet thrust T has been calculated for a perfect gas with $\gamma = 1.4$ from

$$T = [2rd(1.27\ Po_j - P_i) \sin\varphi \cos\eta]$$

where φ = semispan angle (No question of proper nondimensionalization occurs, and "per unit span" values from 2D flows can be compared directly with "total" values from 3D flows in terms of this ratio).

Note that the 2-D value, i.e., the maximum value, for the thrust is used. This value is obviously greater than the value which would be obtained over a span of 30° or more, so that the ratio C_{N_A}/C_{N_R} reflects the real gain according to the input energy used. The amplification ratios obtained in the present experiments are shown in Fig. 11 for the forces measured up to the slot and in Fig. 12 for the forces over the entire cone surface. The latter figure shows again a good agreement between data obtained by integrating the pressure distributions and data obtained from balance measurements. Since the thrust coefficient is a linear function of the jet mass flux ratio $P_{0_j}d/P_{0_\infty}L$ for $P_i \ll P_{0_j}$ i.e.,

$$C_{N_R} = 2.54Lr \sin\varphi \cos\eta \left(\frac{P_{0_j}d}{P_{0_\infty}L}\right) \Big/ \gamma/2M_\infty^2 \left(\frac{P_\infty}{P_{0_\infty}}\right) A_{\text{ref}}$$

it follows that a linear behavior of the normal force coefficient C_{N_A} implies a constant value of the amplification ratio for various jet mass flux ratios. Spaid and Zukoski[10] argue that this is the correct result for purely 2-D flows, and that the decrease in amplification ratio with increasing jet mass flux is due to end-effects (i.e., crossflow) that arise as the jet aspect ratio b/h decreases. The fact that the present data, which are clearly dominated by "end effects," exhibit a nearly constant amplification ratio, or a least no steeper rate of de-

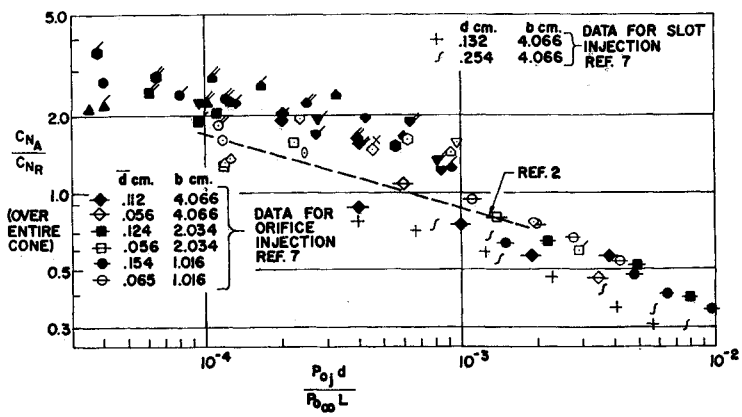

Fig. 12 Normal force amplification ratio, measured over the entire cone surface.

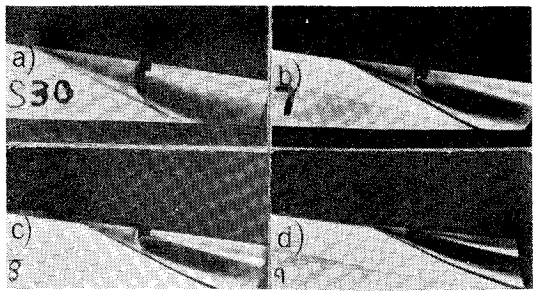

Fig. 13 Schlieren photographs of interaction flowfield with finite-span fences of various heights: a) P_{o_∞} = 1800 psia; h = 3/4 in., b) P_{o_∞} = 1800 psia; h = 1/2 in; c) P_{o_∞} = 1800 psia; h = 3/8 in; and d) P_{o_∞} = 1800 psia; h = 1/4 in.

crease than 2-D results,[2] is therefore particularly interesting. The implication is, of course, that the "losses" due to end-effects in a 2-D flow are not lost at all, and indeed a favorable interference between the crossflow and mainstream occurs downstream of the jet slot. A lift amplification ratio may be defined as

$$C_L/C_R = (C_{N_A} + C_{N_R})/C_{N_R}$$

It can be then seen from Figs. 11 and 12 that the lift coefficient for the cone has been amplified by a factor of about 1.9 due to the interaction force acting up to the slot, and about 3 considering the interaction over the entire cone. The only other available data for a cone are those of Ref. 7. However, the slot was located at the end of the model, and therefore no favorable contribution resulted for the region to the rear of the slot. Included in Fig. 11 are the results of Ref. 7 for various span ratios, and compared to the present experimental results up to the slot. It is clearly seen that they agree satisfactorily, and are lower than the results for the entire cone as presented in Fig. 12.

A heuristic explanation of the nature of the beneficial interaction between the crossflow and the freestream can be made by examining the expression for the normal force coefficient

$$C_{N_A} = \int_A (P - P_i) \cos\varphi \cos\eta dA/\tfrac{1}{2}\rho_\infty U_\infty{}^2 A_{\text{ref}}$$

The integration of the variation of the pressure from its undisturbed value is performed over the entire cone surface. The separated flow region has been considerably extended due to the crossflow and, therefore, the area of integration is much larger than the reference sector area.

In order to account for the crossflow, which extends the interaction region beyond the span of the injection region, one must take into account the reduced penetration height of the jet along the slot span, due to the crossflow. For instance, the experiments of Ref. 2, which were not exactly 2D, must have resulted in a reduced penetration height at the center of the model where the measurements were taken. In order to account for this, it is recommended here that an effective span wider than the slot length be used in the correlation. For example, if the distance between the side plates is B, and the slot span is b, the normal force coefficient obtained for a value of the jet mass flux parameter $P_{0_j}d/P_{0_\infty}L$ should be correlated in terms of a reduced jet mass flux

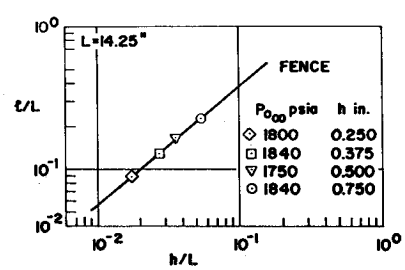

Fig. 14 Separation distance for finite-span fences.

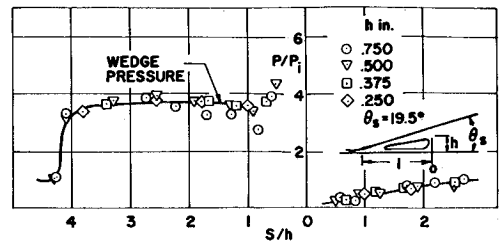

Fig. 15 Surface pressure distribution along plane of symmetry for finite fences.

parameter; namely

$$[(B + b)/2B](P_{0_j}d/P_{0_\infty}L)$$

Such a correlation may reduce or eliminate the decrease in amplification ratio with increasing jet mass flux in nearly 2-D flows.

C. Separation Length Dependence on L

In order to establish the validity of L as a nondimensionalizing quantity, additional tests were performed where the distance from the cone apex to the slot was halved, i.e., from L = 14.25 in. to L = 7.12 in., and the separation distance l and the jet penetration height h vs $P_{0_j}d/P_{0_\infty}L$ were plotted. The resulting experimental points fell exactly on the respective experimental curves plotted in Fig. 6. This shows that the curves of Fig. 6 in 3D are valid, regardless of the choice of L, i.e., regardless of the slot location.

D. Experimental Results: Transverse Fences

In this part of the investigation, the interaction is studied for finite-span fences, of a span angle of 60°. Figs. 13a–13d present the Schlieren photographs for finite-span steps of h = $\frac{3}{4}$ in., $\frac{1}{2}$ in., $\frac{3}{8}$ in., and $\frac{1}{4}$ in. The location of the separation line for h = $\frac{1}{4}$ in. is shown in Fig. 5. It is of interest to note that the separation region has a geometric similarity analogous to the 2-D case. The value of l/h has been measured from the present Schlieren photographs, for the various step heights. Values of l/h of 4.26, 4.3, 4.35, and 4.2 were obtained for the aforementioned finite-span fence heights. These values compare to a value of 4.3 for the 2-D case.[3] In addition, the angle of the separation shock as well as the plateau pressure reached is given by the equivalent wedge angle of 13.1°, which is in quite good agreement with the value obtained in the 2-D case. The separation distance and the pressure distributions for all the above conditions are presented in Fig. 14 and 15. The results have been correlated in terms of S/h, and it is seen that there is good agreement for all the tests. However, one may also observe that, unlike the case of the slot injection, the pressure in the wake region of the fence has no overshoot and in fact is always below the undisturbed conical pressure, thus resulting in an unfavorable interaction at the centerline of the body. However, pressure away from the plane of symmetry of the fence recovered and was above the undisturbed conical value.

The pressure along the centerline in the wake of the fence recovers completely at an S/h of 3. The normal force for interaction was calculated by integrating the entire pressure distribution over the model. The values of $F_i/P_i hb$ obtained in these tests are plotted in Fig. 16. These values include

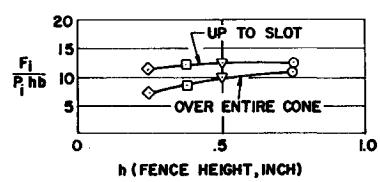

Fig. 16 Normal force parameter for finite fences.

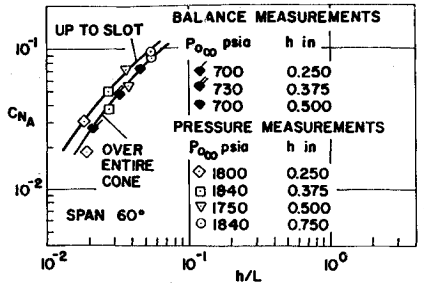

Fig. 17 Normal force coefficient for finite fences.

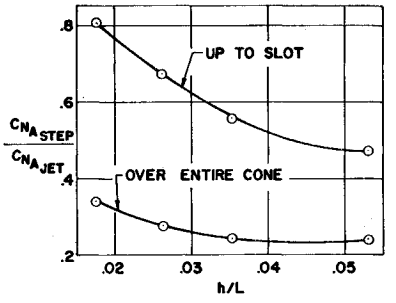

Fig. 18 Ratio of normal force coefficients due to fence and to jet of equivalent height.

the interaction upstream and downstream of the fence. An average value of $F_i/P_i hb$ of 11 was obtained for an M_c of 5.3. The value corresponding to the same conditions for the 2-D interaction as calculated from the correlations of Ref. 3 [Eq. (2)] is 11.2. It is pointed out again here that normal forces which are obtained by integrating the centerline pressure distribution are misleading in the 3-D case; the full span of the separation region, beyond the boundary of the fence, must be included. The normal force coefficient C_{N_A} obtained from the pressure distribution and from balance measurements is plotted in Fig. 17 as a function of the penetration height, and the agreement is remarkable. As in the case of the jet injection, at $h/L > 3 \times 10^{-2}$ which corresponds to $P_{0_j}d/P_{0_\infty}L > 10^{-3}$, the rate of increase of C_{N_A} with penetration height decreases, since the separated region goes beyond $\varphi = 90°$ and therefore, has a counteracting effect.

It may be of interest to compare the interaction obtained from the step to the one obtained from the jet for the same value of h. The results of the jet interaction indicated that the same penetration height was obtained in the present experiments as in the 2-D experiments when 3 to 4 times the amount of mass flow was injected through the slot. However, this resulted (approximately) in $(C_{N_A})_{3D1}(C_{N_A})_{2D} = 3$. In other words, the value of C_{N_A} was approximately the same as in the 2-D case for the same mass flow. In the case of the fence, there is an unfavorable interference due to the pressure downstream of the fence which is below the undisturbed cone value that results in a smaller normal force with an equivalent penetration height h as shown in Fig. 18.

It has been indicated in the literature that a true 2-D separation is hard to achieve, and therefore the separation point is sensitive to crossflow gradients. For this purpose, a 2-D separation is studied on an axially symmetric configuration by placing a full-span fence (or ring) over the surface of the body. For this type of configuration, a more realistic comparison may be made between finite and infinite fences. The results with the full ring are presented in Ref. 14.

III. Conclusions

The interaction of a finite-span, transverse jet on a 7° cone in an $M_\infty = 5.8$ stream has been studied experimentally. Pressure distributions have been measured over the surface of the cone, balance measurements have been taken, separation lines have been determined by injecting ink on the surface, and the structure of the flowfield has been recorded on Schlieren photographs. In addition, an optimization of the interaction span resulted in a maximum favorable value for a slot span of 60° for this configuration. Based on these observations, it has been concluded that along the plane of symmetry the separated region upstream of the jet correlated very well with quasi 2-D experiments in terms of the jet penetration height as the basic scale length. (The aspect ratio of the jet plume b/h is of order 6 or larger. The quasi-two-dimensional behavior will probably diminish as the aspect ratio is decreased). However three times the jet mass flux is required in the case of the finite-span jet to obtain the same jet penetration height as an infinite span (two-dimensional) jet. But the remarkable feature of the three-dimensional phenomenon is that integration of the pressure distribution over the cone surface shows that the normal force coefficient obtained is the *same* as the normal force coefficient per unit span of a 2-D jet with the *same* jet mass flux. This behavior is attributed to a favorable interaction between the crossflow and the main stream that increases the effective span of the jet. It is clearly misleading to consider only the pressure distribution along the centerline when crossflow may be present (although small) due to end effects. If correlated in terms of the jet penetration height, rather than mass flux, the total normal force coefficient of a finite-span jet exceeds the normal force per unit span coefficient of a 2-D jet. The results also indicate a clear favorable interference obtained for the region to the rear of the slot, which could result in as much as 70% increase in the amplification factor. When the jet is replaced by a transverse fence, the 2-D and 3-D normal forces are comparable. It is also noted, however, that a larger low pressure region occurs behind the fence than behind the jet plume, so the net interaction force due to the jet is relatively larger than that due to the fence.

References

[1] Maurer, F., "Three-Dimensional Effects in Shock-Separated Flow Regions Ahead of Lateral Controls-Jets Issuing from Slot Nozzle of Finite Length," *Separated Flows*, AGARD Conference Proceedings IV, May 1966, pp. 597–634.

[2] Sterrett, J. R. and Barger, J. B., "A Theoretical and Experimental Investigation of Secondary Jets in a Mach 6 Free Stream with Emphasis on the Structure of the Jet and Separation Ahead of the Jet," *Separated Flows, Pt. II*, AGARD Conference Proceedings IV, May 1966, pp. 667–700.

[3] Zukoski, E. E., "Turbulent Boundary Layer Separation, in Front of a Forward Facing Step," *AIAA Journal*, Vol. 5, No. 10, Oct. 1967, pp. 1746–1753.

[4] Simpkins, P. G., "Hypersonic Interactions About a Slender Cone Induced by Radial Mass Injection," *Hypersonic Boundary Layers and Flow Fields*, AGARD Conference Proceedings 30, May 1968, pp. 17–14.

[5] Spring, D. J., Street, T. A., and Amick, J. L., "Transverse Jet Experiments and Theories—A Survey of the Literature," RD-TR-67-4, June 1967, U.S. Army Missile Command, Redstone Arsenal, Ala.

[6] Barnes, J. W., Davis, J. G., and Tang, H. H., "Control Effectiveness of Transverse Jets Interacting with a High Speed Free Stream," AFFDL-TR-67-90, I, Sept. 1967, Air Force Flight Dynamics Lab., Wright-Patterson Air Force Base, Ohio.

[7] Barber, J. and Staylor, R., "Investigation of Secondary Jets on a Cone at a Mach Number of 6," *Journal of Spacecraft and Rockets*, Vol. 3, No. 10, Oct. 1966, pp. 1554–1555.

[8] Sterrett, J. R. et al., "Experimental Investigation of Secondary Jets from Two-Dimensional Nozzles with Various Exit Mach Numbers for Hypersonic Control Application," TN-D-3795, Jan. 1967, NASA.

[9] Zukoski, E. E. and Spaid, F. W., "Secondary Injection of Gases into a Supersonic Flow," *AIAA Journal*, Vol. 2, No. 10 Oct. 1964, pp. 1689–1696.

[10] Spaid, F. W. and Zukoski, E. E., "A Study of the Interaction of Gaseous Jets from Transverse Slots with Supersonic Streams," *AIAA Journal*, Vol. 6, No. 2, Feb. 1968, pp. 205–211.

[11] Kaufman, L. G., II et al., "Review of Hypersonic Flow Separation and Control Characteristics," ASD-TDR-62-168, March 1962, Grumman Aircraft Engineering Corp., New York.

[12] Werle, M. J., "A Critical Review of Analytical Methods for Estimating Control Forces Produced by Secondary Injection," NOLTR 68-5, Jan. 1968, United States Naval Ordnance Lab., White Oak, Md.

[13] Hawk, N. E. and Amick, J. L., "Two-Dimensional Secondary Jet Interaction with a Supersonic Stream," *AIAA Journal*, Vol. 5, No. 4, April 1967, pp. 555–660.

[14] Zakkay, V., Erdos, J., and Calarese, W., "An Investigation of the Interaction Between a Transverse Sonic Jet and a Hypersonic Stream," NYU AA-68-27, Aug. 1968, Aerospace Labs., New York University, N.Y.

APRIL 1971 AIAA JOURNAL VOL. 9, NO. 4

Second-Order Longitudinal Curvature Effects in Compressible Laminar Boundary Layers

WILLIAM F. VAN TASSELL*
University of Illinois, Urbana, Ill.

AND

DALE B. TAULBEE†
State University of New York at Buffalo, Buffalo, N. Y.

A study of compressible laminar boundary-layer flow, including second-order longitudinal surface curvature effects, is presented in this paper. The main objective of this research was to determine the structure of the boundary-layer flowfield when longitudinal curvature effects are significant. The remaining second-order effects are not considered in this paper. The governing boundary-layer flow equations are derived from the Navier-Stokes equations by an order of magnitude analysis in which terms of order $Re^{-1/2}$ are retained. A particular class of transformations, based on similarity variables, is then employed in an attempt to obtain a set of total differential equations. Locally similar solutions are then found numerically by a shooting method developed by Smith and Clutter. At low subsonic Mach numbers, both the skin-friction and heat-transfer rates decrease as the curvature increases. However, at supersonic Mach numbers, the curvature may result in an increase in skin-friction and heat-transfer rates.

Nomenclature

C_f = skin friction coefficient, Eq. (35)
f = nondimensional stream function
G = total enthalpy ratio, H/H_E
g = transformation variable, Eq. (25)
H = total enthalpy
$\mathcal{K}$ = metric factor, $= 1 + Ky$
M = Mach number
N = $\rho\mu$ ratio, Eq. (21)
p = pressure
$\bar{p}$ = pressure ratio, p/p_E
P_r = Prandtl number
Re = Reynolds number
S = shear parameter, Eq. (37)
S_t = Stanton number, Eq. (36)
T = temperature
u = x velocity
v = y velocity
x = coordinate on body surface
y = coordinate normal to body surface
α = curvature gradient parameter, Eq. (24)
β = pressure gradient parameter, Eq. (23)
γ = specific heat ratio
δ = boundary layer thickness
δ^* = displacement thickness, Eq. (33)
δ_M = momentum thickness, Eq. (34)
η = transformed y variable, Eq. (15)
θ = density ratio, ρ_E/ρ
κ = curvature
λ = thermal conductivity
μ = ordinary viscosity coefficient, Eq. (9)
μ' = second viscosity coefficient
ξ = transformed x variable, Eq. (25)
ρ = density
τ = shear stress tensor component, Eq. (8)
Ω = curvature parameter, Eq. 22

Subscripts

1 = inviscid flow variable at surface
E = general inviscid flow variable
w = viscous flow variable at surface
x = denotes $\partial/\partial x$
η = denotes $\partial/\partial\eta$
ξ = denotes $\partial/\partial\xi$

Received March 13, 1970; revision received November 23, 1970.

* Assistant Professor, Aeronautical and Astronautical Engineering Department, University of Illinois, Urbana, Illinois; formerly with Cornell Aeronautical Laboratory, Buffalo, New York.

† Associate Professor, Department of Engineering Science, State University of New York at Buffalo, Buffalo, N. Y. Member AIAA.

I. Introduction

MODERN flight vehicle systems have to be designed to operate in a wide variety of altitude and velocity regimes. Typical current systems include re entry vehicles flying at IRBM and ICBM velocities, Apollo-type vehicles entering the earth's atmosphere at lunar return velocity, and high altitude research aircraft such as the X-15. Planetary probes and reusable shuttle craft are now being studied. A wide variety of flight regimes and flight conditions must be considered in order to design such systems successfully.